NANO LETTERS
Letter
Cite This: Nano Lett. XXXX, XXX, XXX−XXX
pubs.acs.org/NanoLett

Dynamic Control of Nanocavities with Tunable Metal Oxides

Jongbum Kim,[†,∥] Enrico G. Carnemolla,[‡] Clayton DeVault,[§] Amr M. Shaltout,[†] Daniele Faccio,[‡] Vladimir M. Shalaev,[†] Alexander V. Kildishev,[†] Marcello Ferrera,[‡] and Alexandra Boltasseva*[,†]

[†]School of Electrical and Computer Engineering and Birck Nanotechnology Center, Purdue University, West Lafayette, Indiana 47907, United States

[‡]Institute of Photonics and Quantum Sciences, Heriot-Watt University, SUPA, Edinburg, Scotland EH14 4AS, United Kingdom

[§]Department of Physics and Astronomy and Birck Nanotechnology Center, Purdue University, West Lafayette, Indiana 47909, United States

[∥]Institute for Research in Electronics and Applied Physics, University of Maryland, College Park, Maryland 20742, United States

Supporting Information

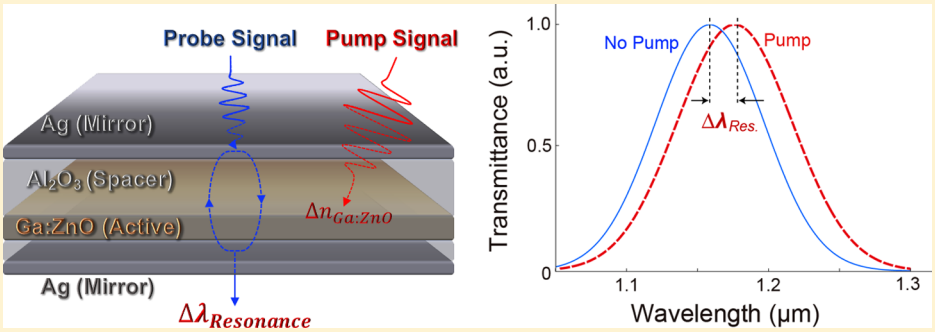

ABSTRACT: Fabry−Pérot metal−insulator−metal (MIM) nanocavities are widely used in nanophotonic applications due to their extraordinary electromagnetic properties and deeply subwavelength dimensions. However, the spectral response of nanocavities is usually controlled by the spatial separation between the two reflecting mirrors and the spacer's refractive index. Here, we demonstrate static and dynamic control of Fabry−Pérot nanocavities by inserting a plasmonic metasurface, as a passive element, and a gallium doped-zinc oxide (Ga:ZnO) layer as a dynamically tunable component within the nanocavities' spacer. Specifically, by changing the design of the silver (Ag) metasurface one can "statically" tailor the nanocavity response, tuning the resonance up to 200 nm. To achieve the dynamic tuning, we utilize the large nonlinear response of the Ga:ZnO layer near the epsilon near zero wavelength to enable effective subpicosecond (<400 fs) optical modulation (80%) at reasonably low pump fluence levels (9 mJ/cm^2). We demonstrate a 15 nm red shift of a near-infrared Fabry−Pérot resonance ($\lambda \cong 1.16\ \mu$m) by using a degenerate pump probe technique. We also study the carrier dynamics of Ga:ZnO under intraband photoexcitation via the electronic band structure calculated from first-principles density functional method. This work provides a versatile approach to design metal nanocavities by utilizing both the phase variation with plasmonic metasurfaces and the strong nonlinear response of metal oxides. Tailorable and dynamically controlled nanocavities could pave the way to the development of the next generation of ultrafast nanophotonic devices.

KEYWORDS: *Metal oxides, nano cavity, pump−probe, epsilon near zero, modulator*

Nanophotonic devices overcome the diffraction limit via locally confining electromagnetic fields and enable approaches to manipulate light on deeply subwavelength scales.[1,2] Recently, a growing interest in the active control of nanophotonic devices has led to the development of low-power reconfigurable and ultracompact switching devices.[3−5] Active control of the optical response holds great promise for the next generation of on-chip nanophotonic and optoelectronic devices. Active modulation by means of thermal,[6,7] mechanical,[8,9] electrical,[4,10−12] and optical tuning[13−17] has already been reported. These strategies have successfully demonstrated the potential of dynamic modulation; however, many approaches are limited by low switching speed and/or high power consumption.

The longstanding interest in the efficient control of large and ultrafast optical nonlinearities has recently made degenerate semiconductors, such as the transparent conducting oxides (TCOs) indium tin oxide (ITO),[13,18−21] aluminum-doped zinc oxide (Al:ZnO),[22−24] and indium-doped cadmium oxide (ICO),[25] extremely attractive for dynamic nanophotonic devices. In fact, these compounds, when operating close to

Received: September 13, 2017
Revised: December 14, 2017
Published: December 28, 2017

DOI: 10.1021/acs.nanolett.7b03919
Nano Lett. XXXX, XXX, XXX−XXX

their epsilon near zero (ENZ) wavelength where the real part of the permittivity has a crossover from the positive to the negative,[26,27] have proven to overcome the typical trade-off between amplitude and speed of their nonlinear response.[18,20,23] Optical tuning of metal oxides triggered by photocarrier excitation has been successfully demonstrated with various geometries and materials[20,22,25] and incorporated in plasmonic systems.[13,19] However, a practical approach to design actively tunable devices by adopting metal oxides into conventional nanophotonic devices has not been reported yet.

Here, we demonstrate all-optical tuning of a metal nanocavity embedded with a TCO thin film (thickness < $\lambda/17$) to achieve the ultrafast spectral tuning of a Fabry–Pérot resonance in the NIR excited near the ENZ wavelength. Metal–insulator–metal (MIM) configurations have been extensively studied in photonics and plasmonics due to their strong light-matter interaction within subwavelength dimensions.[28,29] Simple design and ease of fabrication make MIM structures common in nanophotonics, as evident from the large volume of demonstrations such as negative index metamaterials,[30] beam splitter,[31,32] sensor,[33,34] absorber,[35,36] waveguide,[37,38] nanofocusing,[39] filters,[40,41] nanolasers,[42,43] and polarizer.[12,44] Thus, far, dynamic tuning of MIM-based devices has not been demonstrated. Although electrically driven active absorption tuning in the mid-infrared has been accomplished with ITO embedded MIM metafilms, the demonstrated switching speed was limited by the device capacitance.[12] In comparison with electrical control, intraband pumping on TCOs embedded metal nanocavity offers a large optical modulation under relatively modest fluences (9 mJ/cm^2) and ultrafast THz switching speed (>2.5 THz).[21,24] We observe that Fabry–Pérot resonance in an optical cavity can be transiently red-shifted to enable ON/OFF modulation of the transmitted signal up to 80%. Along with dynamic tuning of nanocavities, we present a versatile method to design the nanocavity resonance with a metasurface.[45] We design the embedded metasurface to provide an additional phase to reflected waves such that the round-trip 2π phase accumulation inside the nanocavity is fulfilled. This approach has been reported to realize ultrathin color filter in the visible range.[45] Consequentially, we observe red-shifted cavity resonances far below the conventional $\lambda/2$ cavity dimension minimum. Our work could enable actively controllable devices for beam steering, adaptive color filtering, and dynamic polarization rotation by using a set of diverse resonance modes in MIM configurations at subwavelength scales.

Experiment, Results, and Discussion. The schematic diagram of our silver-based nanocavity with embedded gallium-doped zinc oxide (Ga:ZnO) as an dynamically tunable element is sketched in Figure 1a. In general, a nanocavity composed of two reflecting metal mirrors separated by a dielectric spacer can support Fabry–Pérot resonance under the condition $4\pi nL/\lambda + 2\phi_m \approx 2\pi m$, where L is the thickness of the cavity ($L_{Al_2O_3\_top} + L_{Al_2O_3\_bottom} + L_{Ga:ZnO}$), n is the refractive index of spacer, ϕ_m is the reflection phase-shift at the interface between metal and dielectric spacer as indicated in Figure 1a, and λ is the effective wavelength. Therefore, with the introduction of a metal oxide, the resonance of the nanocavity can be modulated by $\Delta n_{Ga:ZnO} L_{Ga:ZnO}$, where $\Delta n_{Ga:ZnO}$ is an induced change in the refractive index of Ga:ZnO ($\Delta n_{Ga:ZnO}$) under intraband pumping and $L_{Ga:ZnO}$ is the thickness of Ga:ZnO layer. The optical properties of Ga:ZnO thin film were first characterized

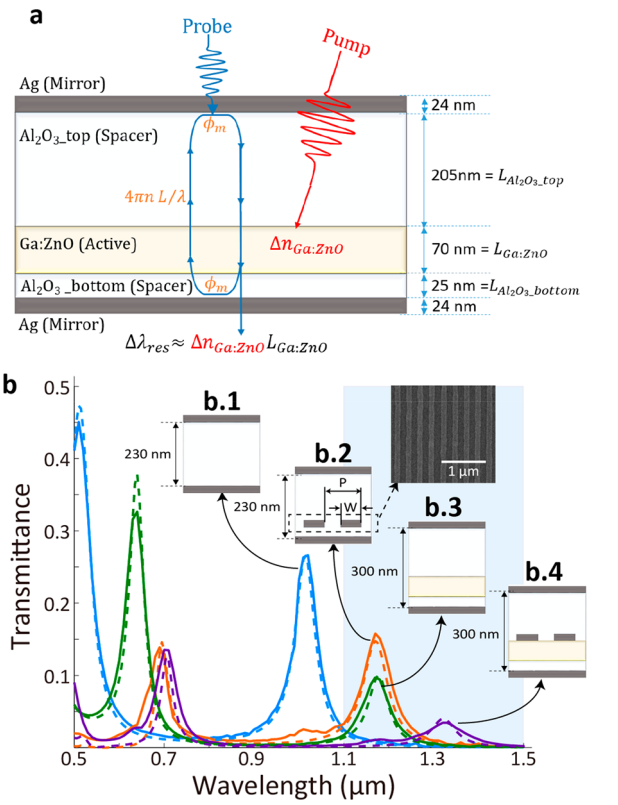

Figure 1. (a) Cross-sectional schematic of the Ga:ZnO embedded nanocavity. The thickness of both top and bottom Ag mirror is 24 nm, total thickness of alumina is 230 nm and the thickness of Ga:ZnO is 70 nm. The reflection phase-shift from metal mirrors (ϕ_m) and phase-shift from cavity ($4\pi nL/\lambda$) are indicated. (b) Experiment (solid line) and simulation (dashed line) of transmission spectra of nanocavity with four different geometries. (b.1) Normal nanocavity. (b.2) Nanocavity with Ag metasurface. P and W is the periodicity and line width of Ag metasurface. (Inset: top view of FE SEM image of fabricated Ag metasurface). (b.3) Nanocavity with Ga:ZnO film. (b.4) Nanocavity with both Ag metasurface and Ga:ZnO film. Spectral region of probe tunability is shaded with a gray rectangle.

by spectroscopic ellipsometry measurements (see Methods). To attain a near-infrared (NIR) Fabry–Pérot resonance in proximity to the ENZ wavelength of Ga:ZnO, the thickness of Ag, aluminum oxide (Al_2O_3), and Ga:ZnO were set at 24, 230, and 70 nm, respectively. Ga:ZnO is spaced 25 nm from the bottom Ag reflecting mirror to maximize the overlap of the Ga:ZnO layer and the internal electric field. The filling ratio of Ga:ZnO to Al_2O_3 is carefully optimized to have a high-transmitted signal at the NIR resonance which can be suppressed by the intrinsic optical loss of Ga:ZnO (see Supporting Information S1).

In addition, we prepare the nanocavities with Ag metasurface to control the cavity resonance without changing the vertical dimension. The design of our metasurface nanocavity is sketched in the inset of Figure 1b.2. Here, the resonance condition of the nanocavities can be modified as $4\pi nL/\lambda + 2\phi_m + \phi_{ms} \approx 2\pi m$ where ϕ_{ms} is the phase-shift induced by the metasurface.[45] The additional phase-shift from metasurface induces the red shift of cavity resonance to satisfy the resonance condition. We find that the resonant wavelength is dependent on the metasurface's lateral dimensions which provides an additional degree of freedom for controlling the resonant wavelength beyond the conventional adjustment of cavity

DOI: 10.1021/acs.nanolett.7b03919
Nano Lett. XXXX, XXX, XXX–XXX

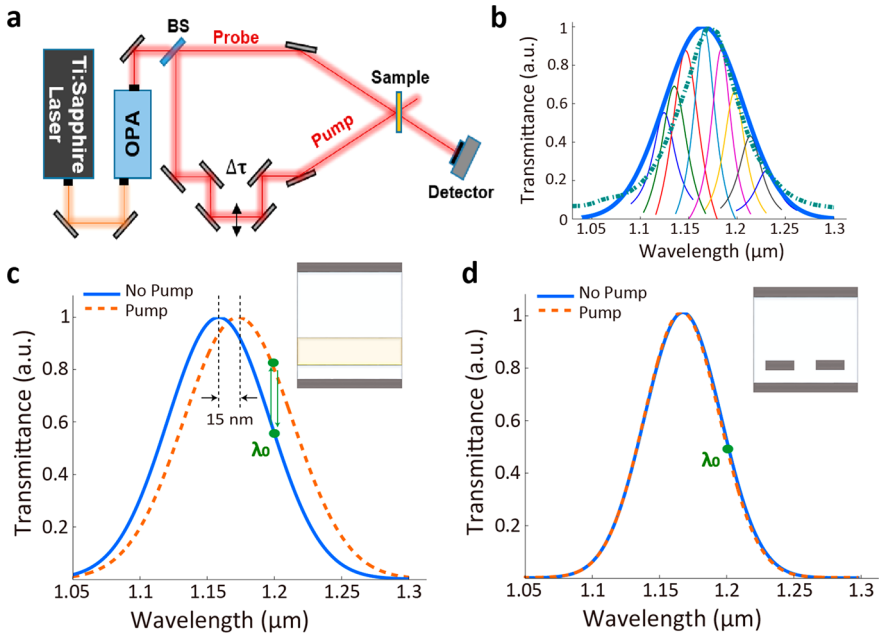

Figure 2. (a) Pump and probe setup. (b) Normalized Gaussian fit (orange line) of the Lorentzian maxima representing the probe pulse is compared to the resonance (green dashed line) measured by ellipsometry on the nanocavity with Ga:ZnO and without a metasurface. For the sake of clarity only few spectra are shown. (c) Normalized resonance shift of about $\Delta\lambda$ = 15 nm of the nanocavity with 70 nm Ga:ZnO film and under pump excitation of intensity I = 9 mJ/cm^2. (d) Normalized resonance of the nanocavity with W = 65 nm and P = 125 nm Ag metasurface under pump excitation of intensity I = 90 GW/cm^2, no resonance shift displayed.

thickness (see Supporting Information S3). As shown in Figure 1b, the nanocavity with a continuous 230 nm thick Al_2O_3 spacer (Figure 1b.1) supports the first order Fabry–Pérot resonance at the wavelength of 1.01 μm. By inserting the 70 nm Ga:ZnO film (Figure 1b.3), the resonance is red-shifted to the wavelength of 1.16 μm due to the increase of the overall cavity thickness. For static tuning with metasurface (Figure 1b.2), the width (W) and periodicity (P) of the nanocavities are set to 65 and 125 nm, respectively; these dimensions were chosen to shift the first order Fabry–Pérot resonance to 1.16 μm. Consequentially, we compensate the 150 nm resonance shift by the introduction of the Ag metasurface to match the resonance of both nanocavities with the metal oxide and the metasurface. Nanocavities with metasurface are also essential for comparing the separate transient contributions from the Ag and Ga:ZnO layer because Ag can also contribute to the optical modulation via NIR free-carrier absorption. All samples were fabricated at the same time and the vertical dimensions of all nanocavities are identical except for the introduction of the Ga:ZnO layer. The supporting document contains more details about the fabrication. Lastly, we observe that the resonance in the nanocavities embedded with both the metal oxide layer and the metasurface (Figure 1b.4) is red-shifted, similar to our observations of inserting metasurfaces into normal nanocavities. This indicates that the introduction of metasurfaces can be applicable to the design of active devices, maintaining the subwavelength scale of nanocavities.

We investigate the tunability of our devices using a pump–probe setup as depicted in Figure 2a. The output of a 100 Hz Ti/sapphire laser (λ_{TS} = 787 nm; $\tau \approx$ 100 fs) is fed into a Topas optical parametric amplifier (OPA) to produce a broad-spectrum pump–probe pulse. The available wavelength tunability range spanned from 1.12 to 1.6 μm (see gray highlight in Figure 1b). A degenerate pump–probe configuration ($\lambda_{probe} = \lambda_{pump}$) was used to evaluate the device dynamics, this was necessary to optimize the coupling of the pump while recording the Fabry–Pérot mode in the NIR range. Initially, the setup was calibrated against the acquired ellipsometry data for the linear case (no pump). For calibration purposes, transmission spectra were recorded for different pulse wavelengths using a Czerny-Turner spectrograph (Andor Shamrock 163 Imaging Spectrographs coupled with an iDus InGaAs detector array). All the acquired curves were then fit with Lorentzian functions whose peaks were finally used to draw the device resonances which were approximated by a Gaussian curve as depicted in the Figure 2b. The characteristic resonances recorded via the two described processes (i.e., ellipsometry and direct transmission of the tuned probe) were the same in within the experimental error. Figure 2c,d reports the transmission spectra with (dashed blue line) and without (solid orange line) optical pumping for both the cavity inclusive of the Ga:ZnO layer and the one with the silver nano-patterning, respectively. As it is evident from Figure 2c,d, an appreciable spectral shift of the cavity resonance was apparent only for the device with the Ga:ZnO layer. This indicates that the photoinduced carrier effects in the Ag mirrors and metasurface were not enough to induce the resonance shift under the same condition of intraband excitation of Ga:ZnO; hence, the induced red shift in resonance of the nanocavity results from the carrier dynamics of the Ga:ZnO film and not from the Ag components. Even though the absolute value of the induced frequency shift is not large if compared to the resonance line width, it is still enough for enabling a remarkable signal modulation when operating in the linear region (see λ_0 point in Figure 2c,d). At this operational wavelength (λ_0 = 1.2 μm) even a small frequency shift can produce a substantial change in the transmitted power (see green arrows Figure 2a).

To record such a modulation and acquire more insights about its nature, we performed a standard degenerate pump and probe experiment at λ_0 = 1.2 μm. The signal transmitted

DOI: 10.1021/acs.nanolett.7b03919
Nano Lett. XXXX, XXX, XXX−XXX

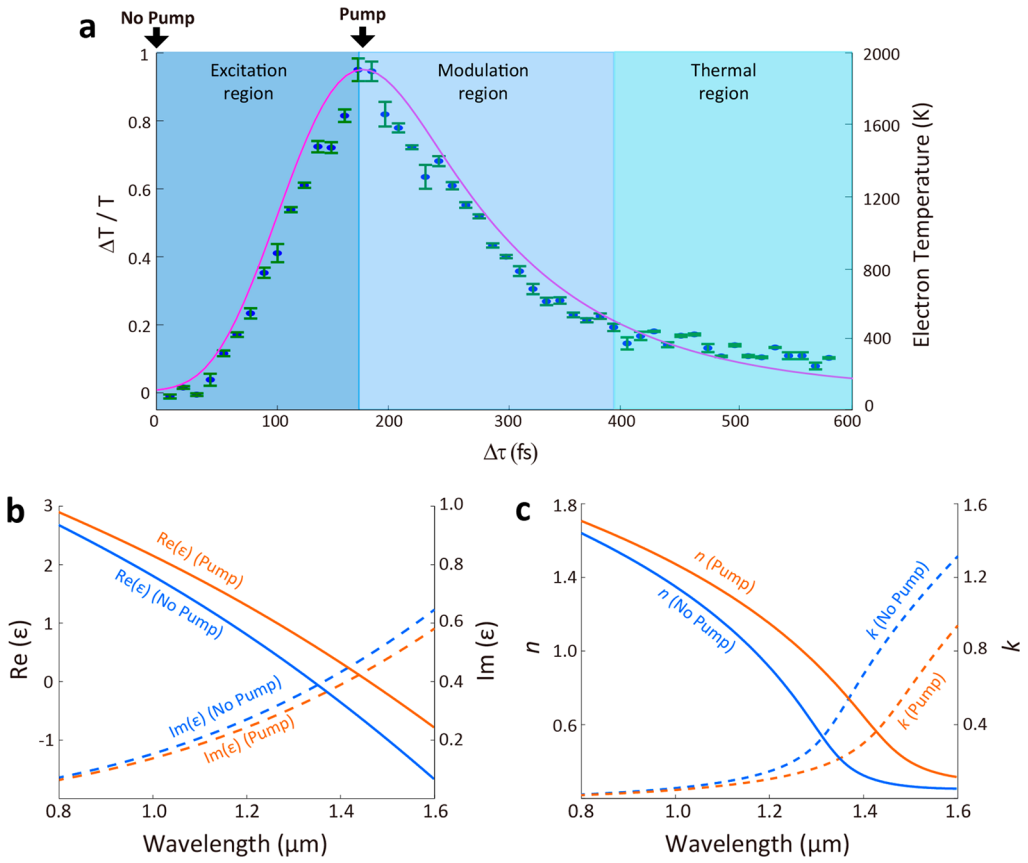

Figure 3. (a) Percentage of the change in transmission as a function of the delay $\Delta\tau$ between the pump and probe pulses in Ga:ZnO embedded nanocavity. Transient dynamics is modeled with two temperature model (pink solid line). Three temporal phases have been identified: rise time, modulation region, and thermal tail. (b) Dielectric functions of Ga:ZnO thin film. Real (solid) and imaginary (dotted) part of permittivity of Ga:ZnO films are extracted by spectroscopic ellipsometry measurement without pump and fitted by numerical simulations with pump. (c) Refractive index of Ga:ZnO films calculated from the extracted dielectric function. Temporal positions for on/off pump states are indicated in panel a.

through the sample was recorded as a function of the time delay $\Delta\tau$ between the pump and the probe. The normalized transient transmissivity is plotted as a function of $\Delta\tau$ in Figure 3a, where three regions can be identified. The first two regions (labeled as "excitation" and "modulation" regions) are equally short and account for an overall ON/OFF time of about 400 fs. A third range, named "thermal" region, is also identified. As shown by the solid pink curves in Figures 3a, the intraband material responses can be successfully modeled using the two-temperature model (TTM) (see Supporting Information). The intraband dynamics of the Ga:ZnO film results in a nonequilibrium hot electrons which relax their excess energy to the lattice via a series of electron−phonon scattering processes, heating the lattice.[46] The decay rate of $\Delta T/T$ was fitted to extract the electron phonon-collision time (τ_{ep}) and found to be τ_{ep} = 212 fs. The long-time constant used for the fitting curve describes a typical slow thermal relaxation process. Excluding slow effects, which only account for a limited fraction of the change in transmission, ≈80% modulation in <400 fs was attained.

The transient change in the optical properties of Ga:ZnO was estimated by fitting the shifted spectral response of the nanocavity with numerical simulation using a commercially available software based on the finite element method (COMSOL Multiphysics) (see Methods). Because the optical response of Ga:ZnO is dominated by the Drude response in the NIR range, we fit the Drude plasma frequency ($\omega_p = \sqrt{\frac{e^2 N_e}{\varepsilon_0 \varepsilon_\infty m_e^* m_0}}$) and damping coefficient ($\Gamma_p = \frac{\hbar e}{m_e^* m_0 \mu_e}$) to match the resonance shift observed by the pump−probe measurement, where N_e is the carrier concentration, m_0 is the mass of electron, m_e^* is the effective mass of electron, and μ_e is the electron mobility. From the extracted ω_p and Γ_p listed in the Table 1, dielectric function and refractive index of Ga:ZnO at two different states are plotted in Figure 3b,c, respectively. We observed that intraband excitation on Ga:ZnO film with 8% light absorption at pump level (9 mJ/cm^2) induces a 130 nm spectral shift of the ENZ wavelength with a small variation (6.5% increment) on damping coefficient. At λ_0 = 1.2 μm, the absolute estimated change in refractive index ($\Delta n_{Ga:ZnO}$) is modest (0.24), while the relative variation ($\Delta n_{Ga:ZnO}/n_{Ga:ZnO}$) is

Table 1. Summary of the Extracted Properties of Ga:ZnO Film[a]

	ω_p (eV)	Γ_p (eV)	μ (eV)	m_e^*	μ_e (cm^2/V·s)
no pump (T_e = 300 K)	1.850	0.0895	3.6803	0.1911	6.770
pump (T_e = 1891 K)	1.700	0.0929	3.5056	0.2263	5.507

[a]This includes plasma frequency (ω_p), the Drude damping coefficient (Γ_p), chemical potential (μ), effective mass (m_e^*), and electron mobility (μ_e).

DOI: 10.1021/acs.nanolett.7b03919
Nano Lett. XXXX, XXX, XXX−XXX

more conspicuous accounting for 26%. As previously reported by using different metal oxides, operating in within the ENZ spectral window gives rise to largely enhanced nonlinearities which are directly responsible for the optical modulation we recorded in our devices.[21,23]

To further analyze the optical response, we compute the carrier distribution of Ga:ZnO in the conduction band under the intraband excitation. The electronic total density of states (TDOS) of 6 wt % doped Ga:ZnO thin film was obtained from first-principles density functional theory (DFT) in our previous study.[47] As the increase of lattice temperature is less than 3 K at the photoexcitation, we do not take the thermal lattice expansion into account. Chemical potential (μ) at pump state is calculated from the assumption that the intraband excitation does not generate extra carriers in the conduction band ($N_{e\_pump} = N_{e\_no\ pump} = 1.176 \times 10^{21}$ cm^{-3}). From the electrical properties of Ga:ZnO thin film measured by hall effect system (MMR Technologies, Inc.) at the room temperature, we calculated the photoinduced change of m_e^* and μ_e. All parameters extracted from calculation are also listed in Table 1. The T_e from TTM model was applied to compute the Fermi–Dirac distribution $f(E,T_e)$ as shown in Figure 4a. The

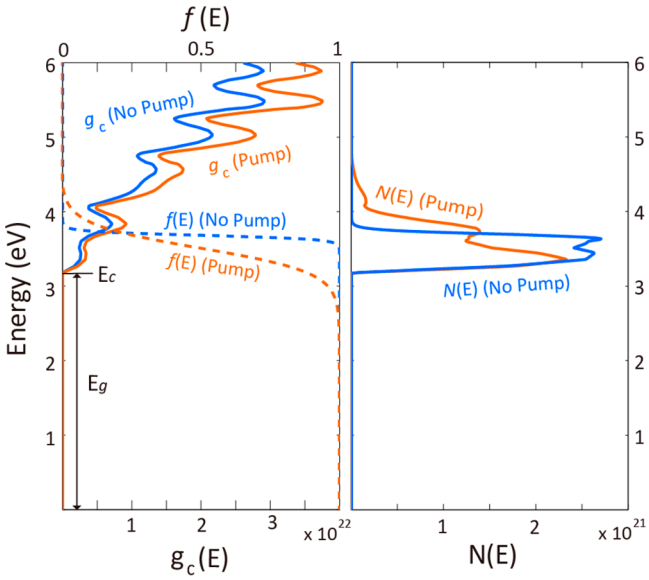

Figure 4. (a) The density of state per unit volume per unit energy $g_c(E)$ and Fermi–Dirac distribution $f(E)$ of Ga:ZnO film. Pump state is estimated from the elevated electron temperature calculated from the TTM model. (b) Carrier distribution of Ga:ZnO thin film calculated by multiplying $g_c(E)$ and $f(E)$. The total number of carrier concentration N_e is the area of carrier distribution.

chemical potential is slightly shifted to lower energy ($\Delta\mu$ = 0.175 eV) and the TDOS per unit volume and per unit energy $g_c(E,T_e)$ is broaden due to the change of m_e^* at the pump state from the relation $g_c(E,T_e) \propto m_e^{*3/2}$. As shown in Figure 4b, the carrier distribution can be simply calculated from the equations $N(E) = g_c(E) \times f(E)$. As the T_e is increased by the phonon–electron interaction, some number of electrons transiently occupy the higher energy levels, which are referred to as hot electrons. This feature explains that the intraband pumping excites free carriers to the hot state and changes the distribution of free electrons in the conduction band. Consequently, the transient change of the motion of electrons (m_e^* and μ_e) in the conduction band modifies electronic band structure, resulting in a change of optical properties of Ga:ZnO dominated by the free carrier interaction with light.

Conclusion. In conclusion, the transient behavior of active nanocavities under IR excitation have been investigated by a degenerate pump and probe technique. By introducing a deeply subwavelength Ga:ZnO thin film ($\lambda/17$) into a classical optical component, we introduce dynamic tuning into an otherwise passive devices. A 15 nm shift in the Fabry–Pérot resonance was recorded together with an ultrafast (<400 fs) ON/OFF modulation of the transmitted signal up to 80%. From the comparison study with oxide-free nanocavity, we identify that the temporal dynamics of active nanocavity result from the nonlinearities of the inserted Ga:ZnO. In addition, we introduce an approach to tailor the cavity resonance by embedding plasmonic metasurface that provides the degree of freedom to design the nanocavities and optical modulators without changing the vertical dimension. Our results pave the way for the design of active nanophotonic devices assisted by TCOs as a dynamic materials platform.

Methods. *Sample Characterization.* The optical properties of 70 nm thick Ga:ZnO films were characterized by variable angle spectroscopic ellipsometry (V-VASE, J.A. Woollam) in the spectral region from 350 to 2500 nm. The dielectric function of the films was retrieved by fitting a Drude–Lorentz oscillator model to the ellipsometry data. The following equation describes the Drude–Lorentz model where the second term comes from the Drude model and the third term represents the Lorentz oscillator

$$\varepsilon(\omega) = \varepsilon_b - \frac{\omega_p^2}{\omega(\omega + i\Gamma_p)} + \frac{f_1\omega_1^2}{\omega_1^2 - \omega^2 - i\omega\Gamma_1}$$

The transmission spectra of fabricated nanocavities were first measured using the spectroscopic ellipsometry. The light source is a xenon lamp with a broadband visible to NIR spectrum. The diameter of the incident beam was set to be 400 μm. The beam sequentially passed through a monochromator, a polarizer, and it is used to expose the sample; then it was collected by a detector. The pump probe measurement was designed to record possible dynamic alterations of a targeted resonance under degenerate pumping. At the beginning, selected resonances were recorded by setting the correspondent polarization and following the calibration process described in the content. Subsequently, output spectra were recorded under degenerate optical pumping where the OPA output wavelength, which was split to produce both the pump (I_{pump} = 90 GW/cm^2) and the probe (I_{probe} = 0.05 GW/cm^2) signals, was tuned across the resonance line width in steps of 5 nm.

Simulations. We validated the experimental spectra with numerical simulations using a commercially available software based on the Finite Element Method (COMSOL Multiphysics). The simulation model is a simplified two-dimensional model with periodic approximations. The periodicity is defined as 150 nm for both a nanocavity with metal oxide layer and a nanocavity with metasurface. The periodic condition is applied to boundary. The index of glass substrate and aluminum oxide are set to 1.50 and 1.76, respectively. The theoretical analysis for nonlinear response was calculated by two temperature models. The supporting document contains more details about the model. By applying the density of state (DOS) calculated by first-principle method (DFT), the carrier distribution of Ga:ZnO at the conduction band was estimated. The

DOI: 10.1021/acs.nanolett.7b03919
Nano Lett. XXXX, XXX, XXX–XXX

Supporting Information contains more details about the calculations.

■ ASSOCIATED CONTENT

Supporting Information

The Supporting Information is available free of charge on the ACS Publications website at DOI: 10.1021/acs.nanolett.7b03919.

Fabrication, design rule, and static control of nanocavities, two temperature model, and electronic band structure for modeling of carrier distribution (PDF)

■ AUTHOR INFORMATION

Corresponding Author

*E-mail: aeb@purdue.edu.

ORCID

Jongbum Kim: 0000-0002-5914-8910

Author Contributions

J.K. and C.D. developed the concept. J.K. carried out the multilayered fabrication of the devices. J.K. performed the linear characterization and E.G.C. performed the pump−probe characterization. J.K., A.S., and A.V.K. developed the numerical simulations for linear response of nanocavities, and J.K. and C.D. developed a two-temperature model for the nonlinear response of Ga:ZnO. J.K. calculated the carrier distribution of Ga:ZnO under the intraband pumping. A.B., A.V.K., V.M.S., D.F., and M.F. oversaw the project and provided the facilities. All the authors contributed and approved the manuscript.

Notes

The authors declare no competing financial interest.

■ ACKNOWLEDGMENTS

This work was supported in part by the Air Force Office of Scientific Research (AFOSR) MURI Grant FA9550-14-1-0389, AFOSR Grant FA9550-14-1-0138, AFOSR Grant FA9550-18-1-0002, and the DARPA Extreme Optics and Imaging (EXTREME) Program. M.F. wishes to acknowledge economic support from the EPSRC (U.K., Grant EP/P019994/1).

■ REFERENCES

(1) Maier, S. A. *Plasmonics: fundamentals and applications*; Springer Science & Business Media, 2007.

(2) Brongersma, M. L.; Shalaev, V. M. The case for plasmonics. *Science* **2010**, *328*, 440−441.

(3) Liu, M.; Yin, X.; Ulin-Avila, E.; Geng, B.; Zentgraf, T.; Ju, L.; Wang, F.; Zhang, X. A graphene-based broadband optical modulator. *Nature* **2011**, *474*, 64−67.

(4) Dionne, J. A.; Diest, K.; Sweatlock, L. A.; Atwater, H. A. PlasMOStor: a metal− oxide− Si field effect plasmonic modulator. *Nano Lett.* **2009**, *9*, 897−902.

(5) MacDonald, K. F.; Zheludev, N. I. Active plasmonics: current status. *Laser Photonics Rev.* **2010**, *4*, 562−567.

(6) Lei, D. Y.; Appavoo, K.; Sonnefraud, Y.; Haglund, R. F., Jr; Maier, S. A. Single-particle plasmon resonance spectroscopy of phase transition in vanadium dioxide. *Opt. Lett.* **2010**, *35*, 3988−3990.

(7) Lopez, R.; Feldman, L. C.; Haglund, R. F., Jr. Size-Dependent Optical Properties of VO_2 Nanoparticle Arrays. *Phys. Rev. Lett.* **2004**, *93*, 177403.

(8) Huang, F.; Baumberg, J. J. Actively tuned plasmons on elastomerically driven Au nanoparticle dimers. *Nano Lett.* **2010**, *10*, 1787−1792.

(9) Ou, J. Y.; Plum, E.; Jiang, L.; Zheludev, N. I. Reconfigurable Photonic Metamaterials. *Nano Lett.* **2011**, *11*, 2142−2144.

(10) Feigenbaum, E.; Diest, K.; Atwater, H. A. Unity-order index change in transparent conducting oxides at visible frequencies. *Nano Lett.* **2010**, *10*, 2111−2116.

(11) Li, Z.; Zhou, Y.; Qi, H.; Pan, Q.; Zhang, Z.; Shi, N. N.; Lu, M.; Stein, A.; Li, C. Y.; Ramanathan, S.; et al. Correlated Perovskites as a New Platform for Super-Broadband-Tunable Photonics. *Adv. Mater.* **2016**, *28*, 9117−9125.

(12) Park, J.; Kang, J.-H.; Kim, S. J.; Liu, X.; Brongersma, M. L. Dynamic Reflection Phase and Polarization Control in Metasurfaces. *Nano Lett.* **2017**, *17*, 407−413.

(13) Abb, M.; Albella, P.; Aizpurua, J.; Muskens, O. L. All-optical control of a single plasmonic nanoantenna−ITO hybrid. *Nano Lett.* **2011**, *11*, 2457−2463.

(14) Jadidi, M. M.; König-Otto, J. C.; Winnerl, S.; Sushkov, A. B.; Drew, H. D.; Murphy, T. E.; Mittendorff, M. Nonlinear Terahertz Absorption of Graphene Plasmons. *Nano Lett.* **2016**, *16*, 2734−2738.

(15) Shcherbakov, M. R.; Liu, S.; Zubyuk, V. V.; Vaskin, A.; Vabishchevich, P. P.; Keeler, G.; Pertsch, T.; Dolgova, T. V.; Staude, I.; Brener, I.; et al. Ultrafast all-optical tuning of direct-gap semiconductor metasurfaces. *Nat. Commun.* **2017**, *8*, 17.

(16) Pacifici, D.; Lezec, H. J.; Atwater, H. A. All-optical modulation by plasmonic excitation of CdSe quantum dots. *Nat. Photonics* **2007**, *1*, 402−406.

(17) Wurtz, G. A.; Pollard, R.; Hendren, W.; Wiederrecht, G. P.; Gosztola, D. J.; Podolskiy, V. A.; Zayats, A. V. Designed ultrafast optical nonlinearity in a plasmonic nanorod metamaterial enhanced by nonlocality. *Nat. Nanotechnol.* **2011**, *6*, 107−111.

(18) Alam, M. Z.; De Leon, I.; Boyd, R. W. Large optical nonlinearity of indium tin oxide in its epsilon-near-zero region. *Science* **2016**, *352*, 795−797.

(19) Abb, M.; Wang, Y.; De Groot, C.; Muskens, O. L. Hotspot-mediated ultrafast nonlinear control of multifrequency plasmonic nanoantennas. *Nat. Commun.* **2014**, *5*, 4869.

(20) Guo, P.; Schaller, R. D.; Ocola, L. E.; Diroll, B. T.; Ketterson, J. B.; Chang, R. P. Large optical nonlinearity of ITO nanorods for sub-picosecond all-optical modulation of the full-visible spectrum. *Nat. Commun.* **2016**, *7*, 12892.

(21) Guo, P.; Schaller, R. D.; Ketterson, J. B.; Chang, R. P. Ultrafast switching of tunable infrared plasmons in indium tin oxide nanorod arrays with large absolute amplitude. *Nat. Photonics* **2016**, *10*, 267.

(22) Kinsey, N.; DeVault, C.; Kim, J.; Ferrera, M.; Shalaev, V. M.; Boltasseva, A. Epsilon-near-zero Al-doped ZnO for ultrafast switching at telecom wavelengths. *Optica* **2015**, *2*, 616−622.

(23) Caspani, L.; Kaipurath, R. P. M.; Clerici, M.; Ferrera, M.; Roger, T.; Kim, J.; Kinsey, N.; Pietrzyk, M.; Di Falco, A.; Shalaev, V. M.; et al. Enhanced Nonlinear Refractive Index in Epsilon-Near-Zero Materials. *Phys. Rev. Lett.* **2016**, *116*, 233901.

(24) Clerici, M.; Kinsey, N.; DeVault, C.; Kim, J.; Carnemolla, E. G.; Caspani, L.; Shaltout, A.; Faccio, D.; Shalaev, V.; Boltasseva, A.; et al. Controlling hybrid nonlinearities in transparent conducting oxides via two-colour excitation. *Nat. Commun.* **2017**, *8*, 15829.

(25) Diroll, B. T.; Guo, P.; Chang, R. P. H.; Schaller, R. D. Large Transient Optical Modulation of Epsilon-Near-Zero Colloidal Nanocrystals. *ACS Nano* **2016**, *10*, 10099−10105.

(26) Engheta, N. Circuits with light at nanoscales: optical nanocircuits inspired by metamaterials. *Science* **2007**, *317*, 1698−1702.

(27) Liberal, I.; Engheta, N. Near-zero refractive index photonics. *Nat. Photonics* **2017**, *11*, 149−158.

(28) Kurokawa, Y.; Miyazaki, H. T. Metal-insulator-metal plasmon nanocavities: Analysis of optical properties. *Phys. Rev. B: Condens. Matter Mater. Phys.* **2007**, *75*, 035411.

(29) Jung, J.; Søndergaard, T.; Bozhevolnyi, S. I. Gap plasmon-polariton nanoresonators: Scattering enhancement and launching of surface plasmon polaritons. *Phys. Rev. B: Condens. Matter Mater. Phys.* **2009**, *79*, 035401.

(30) Shalaev, V. M. Optical negative-index metamaterials. *Nat. Photonics* **2007**, *1*, 41−48.

DOI: 10.1021/acs.nanolett.7b03919
Nano Lett. XXXX, XXX, XXX−XXX

(31) Pors, A.; Albrektsen, O.; Radko, I. P.; Bozhevolnyi, S. I. Gap plasmon-based metasurfaces for total control of reflected light. *Sci. Rep.* **2013**, *3*, 2155.
(32) Bahramipanah, M.; Mirtaheri, S. A.; Abrishamian, M. S. Electrical beam steering with metal-anisotropic-metal structure. *Opt. Lett.* **2012**, *37*, 527−529.
(33) Kim, J.; Dutta, A.; Memarzadeh, B.; Kildishev, A. V.; Mosallaei, H.; Boltasseva, A. Zinc oxide based plasmonic multilayer resonator: Localized and gap surface plasmon in the infrared. *ACS Photonics* **2015**, *2*, 1224−1230.
(34) Wohltjen, H.; Snow, A. W. Colloidal metal− insulator− metal ensemble chemiresistor sensor. *Anal. Chem.* **1998**, *70*, 2856−2859.
(35) Kajtár, G.; Kafesaki, M.; Economou, E.; Soukoulis, C. Theoretical model of homogeneous metal−insulator−metal perfect multi-band absorbers for the visible spectrum. *J. Phys. D: Appl. Phys.* **2016**, *49*, 055104.
(36) Aydin, K.; Ferry, V. E.; Briggs, R. M.; Atwater, H. A. Broadband polarization-independent resonant light absorption using ultrathin plasmonic super absorbers. *Nat. Commun.* **2011**, *2*, 517.
(37) Wen, K.; Hu, Y.; Chen, L.; Zhou, J.; Lei, L.; Guo, Z. Fano Resonance with Ultra-High Figure of Merits Based on Plasmonic Metal-Insulator-Metal Waveguide. *Plasmonics* **2015**, *10*, 27−32.
(38) Verhagen, E.; Dionne, J. A.; Kuipers, L.; Atwater, H. A.; Polman, A. Near-field visualization of strongly confined surface plasmon polaritons in metal− insulator− metal waveguides. *Nano Lett.* **2008**, *8*, 2925−2929.
(39) Choo, H.; Kim, M.-K.; Staffaroni, M.; Seok, T. J.; Bokor, J.; Cabrini, S.; Schuck, P. J.; Wu, M. C.; Yablonovitch, E. Nanofocusing in a metal-insulator-metal gap plasmon waveguide with a three-dimensional linear taper. *Nat. Photonics* **2012**, *6*, 838−844.
(40) Diest, K.; Dionne, J. A.; Spain, M.; Atwater, H. A. Tunable Color Filters Based on Metal− Insulator− Metal Resonators. *Nano Lett.* **2009**, *9*, 2579−2583.
(41) Kim, S.; Man, M.; Qi, M.; Webb, K. J. Angle-insensitive and solar-blind ultraviolet bandpass filter. *Opt. Lett.* **2014**, *39*, 5784−5787.
(42) Noginov, M.; Zhu, G.; Belgrave, A.; Bakker, R.; Shalaev, V.; Narimanov, E.; Stout, S.; Herz, E.; Suteewong, T.; Wiesner, U. Demonstration of a spaser-based nanolaser. *Nature* **2009**, *460*, 1110−1112.
(43) Lu, Y.-J.; Kim, J.; Chen, H.-Y.; Wu, C.; Dabidian, N.; Sanders, C. E.; Wang, C.-Y.; Lu, M.-Y.; Li, B.-H.; Qiu, X.; et al. Plasmonic nanolaser using epitaxially grown silver film. *Science* **2012**, *337*, 450−453.
(44) Pors, A.; Nielsen, M. G.; Bozhevolnyi, S. I. Broadband plasmonic half-wave plates in reflection. *Opt. Lett.* **2013**, *38*, 513−515.
(45) Shaltout, A. M.; Kim, J.; Boltasseva, A.; Shalaev, V. M.; Kildishev, A. V. Ultrathin and Multicolor Optical Cavities with Embedded Metasurfaces. **2017** arXiv:1711.05798.
(46) Gantmakher, V. F. The experimental study of electron-phonon scattering in metals. *Rep. Prog. Phys.* **1974**, *37*, 317.
(47) Kim, J.; Naik, G. V.; Gavrilenko, A. V.; Dondapati, K.; Gavrilenko, V. I.; Prokes, S.; Glembocki, O. J.; Shalaev, V. M.; Boltasseva, A. Optical properties of gallium-doped zinc oxide—a low-loss plasmonic material: first-principles theory and experiment. *Phys. Rev. X* **2013**, *3*, 041037.

DOI: 10.1021/acs.nanolett.7b03919
Nano Lett. XXXX, XXX, XXX−XXX